MODIFIED DESIGN OF A SCALE MODEL OF A CYLINDRICAL ROTOR, STEAM TURBINE GENERATOR

Billy Bryan Williams

MODIFIED DESIGN OF A SCALE MODEL OF A CYLINDRICAL ROTOR, STEAM TURBINE GENERATOR

by

BILLY BRYAN WILLIAMS

B.S., United States Naval Academy
(1964)

SUBMITTED IN PARTIAL FULFILLMENT
OF THE REQUIREMENTS FOR THE
DEGREE OF OCEAN ENGINEER AND
THE DEGREE OF MASTER OF SCIENCE IN
ELECTRICAL ENGINEERING

at the
MASSACHUSETTS INSTITUTE OF
TECHNOLOGY
June, 1972

MODIFIED DESIGN OF A SCALE MODEL OF A CYLINDRICAL ROTOR, STEAM TURBINE GENERATOR

by

BILLY BRYAN WILLIAMS

Submitted to the Department of Ocean Engineering on May 12, 1972 in partial fulfillment of the requirements for the degree of Ocean Engineer and the degree of Master of Science in Electrical Engineering.

ABSTRACT

This thesis is a continuation of work done by the M.I.T. Electric Power Systems Laboratory on a project to build a physical scale model of the American Electric Power Service Corporation Network. Specifically, it is associated with the portion of the project directed toward modeling large steam turbine generators.

The object of this thesis is to redesign a model of the AEP BIG SANDY No. 2 generating unit so as to eliminate excessive eddy current loss characteristics exhibited by the model. The eddy current loss problem in a small gap generator is studied and a design modification, which is to close the rotor and stator slots, is established.

To aid in the modified design, a teledeltos modeling technique is used to investigate the effects of saturation in the model rotor. Finally, procedures are presented to calculate the model leakage reactance in order to determine the amount of external reactance necessary in the armature and field circuits to accurately reproduce the transient and synchronous reactance of BIG SANDY.

THESIS SUPERVISOR: J. L. Kirtley

Title: Assistant Professor of Electrical Engineering

Thesis Reader: W. C. Dietz

Title: Associate Professor of Marine Engineering

ACKNOWLEDGEMENTS

I should like to express my appreciation to Professor J. L. Kirtley for all his assistance and advice during the course of this thesis. Additionally, I thank Professor G. L. Wilson for his support and guidance. Finally, I wish to thank my wife, Rosemary, for typing this thesis report.

The thesis was funded by the American Electric Power Service Corporation and the United States Navy.

TABLE OF CONTENTS

		page
TITLE PAGE		1
ABSTRACT		2
ACKNOWLEDGEMENTS		3
LIST OF FIGURES		5
LIST OF TABLES		6
CHAPTER 1	INTRODUCTION	7
1.1.	History of the Modeling Project	7
1.2	Objective of Thesis	10
1.3	Design Procedure	11
CHAPTER 2	ELIMINATION OF POLE FACE EDDY CURRENT LOSSES	18
2.1	Design Modification to Reduce Eddy Current Loss	18
2.2	Experimental Verification of Loss Reduction Method	26
2.3	No-Load Eddy Current Loss Calculation for Modified Design	30
CHAPTER 3	MODIFIED DESIGN	35
3.1	General	35
3.2	Experimental Prediction of K_{bsat}	35
3.3	Modified Design	39
CHAPTER 4	LEAKAGE REACTANCES	54
4.1	General	54
4.2	Armature Leakage Reactance	54
4.3	Field Leakage Reactance	65
4.4	Estimation of External Reactance Correction for BIG SANDY Model	69
CHAPTER 5	CONCLUSIONS	71
5.1	Modified Design Conclusions and Recommendations	71
5.2	Applicability of Modeling Procedure to Naval Electrical Systems	72
REFERENCES		73

LIST OF FIGURES

		page
Figure 2.1	Variation of Fundamental Tooth-Ripple Flux Density	19
Figure 2.2	Flux Distribution in Umans' BIG SANDY Model	21
Figure 2.3	Traveling Sinusoidal Flux Wave	22
Figure 2.4	No-Load Electrical Loss Test Loss Measurements	28
Figure 2.5	No-Load Electrical Loss Test Flux Measurements	29
Figure 2.6	Air Gap Flux Values Assumed for Loss Calculation	32
Figure 3.1	Teledeltos Model	37
Figure 3.2	Modified Rotor Lamination	46
Figure 3.3	Modified Stator Lamination	47
Figure 3.4	Modified Rotor Tooth and Slot Configuration	49
Figure 3.5	Modified Stator Tooth and Slot Configurations	50
Figure 4.1	Magnetic Paths for Armature Leakage Fluxes	55
Figure 4.2	Slot Dimension for Leakage Calculation	57
Figure 4.3	Air Gap Flux Linkages	62

LIST OF TABLES

		page
Table 1.1	Summary of Scaling Constants	12
Table 2.1	Relative Amplitudes of Harmonics For Various Stator Slot Widths	25
Table 3.1	Scaling Constant Relations	40
Table 3.2	Model Constant Values	41
Table 3.3	BIG SANDY Generator and Model Characteristics	52
Table 3.4	MITCHEL I Generator and Model Characteristics	53
Table 4.1	Properties of Slots Carring Coil Sides From Different Phases for a Balanced Three-Phase Winding	60
Table 4.2	Reactance Calculations in Per Unit	68

CHAPTER 1

INTRODUCTION

1.1. History of the Modeling Project

This thesis is a continuation of work done by the M.I.T. Electric Power Systems Laboratory on a project to build a physical scale model of the American Electric Power Service Corporation Network. Specifically, it is associated with the portion of the project directed toward modeling large steam turbine generators.

A feasibility study of the concept was initiated in January 1967. This study was based upon a magnetostatic model of a generator and illustrated the viability of a physical scale model for transient stability studies in which mathematical models have limited application because of the complexity of electromagnetic and electromechanical phenomena. In order to model these phenomena ideally at an acceptable size and power level, it was proved necessary to construct the model from materials with a much higher electrical conductivity than that normally required.[1]

The required conductivity was obtainable from some pure materials in a cryogenic environment. However, because of the high cost and complexity associated with this procedure, it was determined to be impractical to proceed with physical scale modeling in this way.[2]

Efforts were then directed toward modeling with available materials. The approach was to use a rotor made from a composite of high permeability magnetic material and copper in order to model the transient eddy current decay in a solid rotor forging. The importance of accounting for eddy current phenomena in modeling was

evidenced in field discharge tests made on the BREED No. 1 generator by J. H. Kinghorn which indicated that the effects do not dissipate quickly enough to be ignored as has been assumed in mathematical models.[3]

A procedure to scale eddy current decay was provided by A. S. Pasquale in his study of eddy current transients in a cylindrical rotor resulting from changes in flux in a plane perpendicular to the axis. Pasquale concluded that two constants must be kept the same in the model and full scale generator.[4] These constants are τ and C defined by:

$$\tau = \mu\sigma R_f^2 \tag{1.1}$$

$$C = \frac{\mu}{\mu_o}\left[\frac{\frac{R_a^2}{R_f^2} - 1}{\frac{R_a^2}{R_f^2} + 1}\right] \tag{1.2}$$

where μ = rotor material permeability
σ = rotor material conductivity
R_a = armature inner radius
R_f = rotor radius

The constant, μ, describes the eddy current decay rate in the rotor material, and the constant, C, describes the difference between a magnetic path for flux which crosses the air gap and one which closes in the rotor. It may be written approximately as[5]

$$C \simeq \frac{\frac{\text{Airgap Length}}{\mu_o}}{\frac{R_f}{\mu}} \tag{1.3}$$

Pasquale's analysis assumes linear field behavior. We must consider also the effects of saturation in the rotor in interpreting his results.[6] The initial flux densities in a real machine under operating conditions are near the saturation level of the rotor material. When a transient occurs, saturation in the rotor 90^{o} from the pole face tends to force more flux across the air gap to produce armature voltage. The value of the constant, C, is decreased since it is inversely proportional to the reluctance of the path through the rotor iron which is higher because of saturation. If we assume that saturation does not affect time constants, then the only effect of saturation is to change C. The important point of all this is that if we are going to physically model the transient behavior of a large steam turbine generator, we must reproduce saturation in the model rotor as it occurs in the generator in addition to matching the values of τ and C so that the changes in C because of saturation will occur relatively the same in the model and the generator.

A physical scale model was constructed and tested. It had been designed to model the AEP CARDINAL No. 1 generator but technical difficulties resulted in the model having an air gap which was too large to match the constant C. Field discharge tests were conducted which indicated that the changes in C that occurred in the model were relatively the same as those observed in the BREED tests, i.e., the initial difference in the values of C between the model and BREED accounted for the difference observed in the decay rate of the armature voltage during the tests.

The results of those tests provided the impetus for the design, construction and testing of a new model which scaled the AEP BIG SANDY No. 2 generating unit. BIG SANDY was picked because it has the smallest air gap of the

generators to be modeled and represented the most severe test of the modeling technique. This model was also unsatisfactory, in that it exhibited no-load electrical losses on the order of 50% of rated output. The severity of the losses permitted only limited testing of the model.

1.2. Objective of Thesis.

The primary purpose of this thesis is to redesign the BIG SANDY model to eliminate the no-load eddy current loss characteristics observed in the present model. In Chapter 2, a procedure to eliminate the losses is studied, and a design modification, which is to reduce the stator slot width, is developed. Additionally, the results of an experiment conducted to verify that a reduced stator slot width will solve the loss problem are reported.

The modified design is developed in Chapter 3. A secondary objective of this thesis is to insure that the redesigned rotor and stator laminations may be used to construct models of other of the AEP units. The modified design is thus developed to be applicable to a model of the AEP MITCHEL No. 1 generator in addition to BIG SANDY.

The modeling procedure, which is described in Section 1.3, is oriented toward modeling magnetic diffusion in the rotor of the steam turbine generator. In order to accurately reproduce the transient characteristics of the full size machine in the model, it is necessary to add external reactances in the field and armature circuits of the model to match per unit leakage reactances in the model with those observed in the generator. The problem of calculating the model leakage reactances and making appropriate adjustments is addressed in Chapter 4.

Finally, in Chapter 5, in addition to a listing of

results and conclusions, a brief discussion of the applicability of the modeling procedure to model a shipboard electrical power system is also included.

1.3. Design Procedure

The design procedure which was used to complete the modified design has evolved through a series of reports and theses. It consists of defining scaling constants, (listed in Table 1.1) by the ratio of the parameter for the model relative to that for the real machine, and then developing constraints among these parameters from basic machine relations and Pasquale's results. One of these constraints along with the basic scaling technique was developed in the initial study.[7]

The generator operates as a quasi-static, magnetic field system which may be described by Maxwell's equations as follows:

$$(1.4)\quad \nabla \times \bar{H} = \bar{J} \qquad (1.5)\quad \nabla \times \bar{E} = -\frac{\partial \bar{B}}{\partial t}$$

$$(1.6)\quad \nabla \cdot \bar{B} = 0 \qquad (1.7)\quad \nabla \cdot \bar{J} = 0$$

$$(1.8)\quad \bar{J} = \sigma \bar{E} \qquad (1.9)\quad \bar{B} = \bar{f}(\bar{H})$$

where

$$\nabla = \bar{i}_x \frac{\partial}{\partial x} + \bar{i}_y \frac{\partial}{\partial y} + \bar{i}_z \frac{\partial}{\partial z}$$

$\bar{i}_x$, $\bar{i}_y$, $\bar{i}_z$ are unit vectors in the axis directions

$\bar{H}$ = magnetic field intensity

$\bar{B}$ = magnetic flux density

$\bar{E}$ = electric field intensity

$\bar{J}$ = current density

TABLE 1.1

SUMMARY OF SCALING CONSTANTS

Scaling Factor	Ratio of Property of Model to that of Actual Machine
K_{ℓ}	Rotor radius
$K_{\ell}K_{a\ell}$	Active length of field and armature
K_{μ}	Effective magnetic permeability of rotor
K_{σ}	Effective electrical conductivity of rotor
K_{t}	Turn per cycle
K_{g}	Effective air gap length
K_{v}	Rated armature voltage
K_{n}	Armature series turns per phase
K_{i}	Rated armature current
K_{p}	Power rating
K_{Bsat}	Saturation flux density

The procedure in scaling is to write a separate set of these equations for the model, designated by the subscript m, and for the full scale generator, designated by the subscript s. For instance, using equation (1.8) for the model,

$$\bar{J}_m = \sigma_m \bar{E}_m \tag{1.10}$$

and for the generator

$$\bar{J}_s = \sigma_s \bar{E}_s . \tag{1.11}$$

In order to scale the electromagnetic phenomena described by equations (1.4)-(1.9), we must insure correspondence between each variable in the model with the same variable in the generator. This is accomplished by defining scaling relations for each system variable, i.e.,

$$\bar{J}_m = K_J \bar{J}_s \tag{1.12}$$

$$\sigma_m = K_\sigma \sigma_s \tag{1.13}$$

$$\bar{E}_m = K_E \bar{E}_x \tag{1.14}$$

Similar relations are defined for the other system variables. Constraints among the scaling constants, K_J, K_σ,etc. may be deduced by substituting the scaling relations into the set of equations written for the model and collecting the constants on one side of the equation, i.e., substituting equations (1.12)-(1.14) into equation (1.11), we obtain

$$(1.15)\quad K_J \bar{J}_s = K_\sigma \sigma_s \times K_E \bar{E}_s$$

Collecting the scaling constants on the left side of the equation yields the result

$$(1.16)\quad \frac{K_J}{K_\sigma K_E} \bar{J}_s = \sigma_s \bar{E}_s$$

which indicates that the constaint

$$(1.17)\quad \frac{K_J}{K_\sigma K_E} = 1 \quad \text{must be satisfied in order to}$$

accurately model electromagnetic phenomena. Equivalent operations on equations (1.4)-(1.7) and (1.9) with scaling relations appropriately defined will yield the following additional constraints among the scaling constants:[8]

$$(1.18)\quad \frac{K_E K_t}{K_B K_\ell} = 1$$

$$(1.19)\quad \frac{K_H}{K_\ell K_J} = 1$$

$$(1.20)\quad \frac{\bar{f}_m(K_H \bar{H}_S)}{K_B} = \bar{f}_s(\bar{H}_s)$$

Since the relative effect of the magnetic properties of air in the model and generator must be equal, we must set

$$(1.21)\quad \frac{K_H}{K_B} = 1$$

As a result of this, it is necessary to insure that the magnetization curves for the material used in the model is similar to that for the generator material. This is

indicated by equation (1.20).

We may now combine equations (1.17)-(1.19). The resultant constraint expression is

$$(1.22) \quad K_\sigma K_\mu K_\ell^2 = K_t$$

The development to this point is exact. In order to build a practical model from available materials, we relax the requirement that all dimensions and material properties scale by the same factor throughout the machine. Instead, we use the results of Pasquale's analysis and the subsequent interpretation discussed in Section 1.1. We strive to reproduce electromagnetic diffusion in the rotor by scaling the constant C and in insuring that saturation occurs in the model relatively the same as in the actual machine. This latter requirement is met by imposing the constraint represented by equation (1.22) to the transverse dimension since it is the changes in flux in a plane perpendicular to the rotor axis that affect the eddy current transients that we are attempting to accurately reproduce.[9] From equation(1.3),the constraint imposed by keeping C constant is

$$(1.23) \quad \frac{K_g K_\mu}{K_\ell} = 1$$

In order to keep the length of the model practical, we adjust the length scaling constant by a factor $K_{a\ell}$. Thus, the active length scaling factor is $K_{a\ell}K_\ell$. This is justified on the basis that machine output performance is dominated by actual length, thus allowing a reduction in the dimension so long as we keep $K_{a\ell}$ large enough so that end turn effects do not dominate.[10]

The remaining scaling constant relations may now be developed (Development from Reference 11) from basic machine relations. For scaling constant definitions, refer to table 1.1. The rated armature volts per turn will scale as

$$(1.24) \quad \frac{V}{N} \sim K_{Bsat} K_{\ell}^{2} K_{a\ell}$$

if we keep the pitch and distribution factors constant between the model and actual machine.

The mutual reactance per turn squared is proportional to air gap area and inversely proportional to effective gap length.

$$(1.25) \quad X_{ad} \sim \frac{K_{\ell}^{2} K_{a\ell}}{K_{g}}$$

We wish to keep the machine reactances the same in the model and generator on a per unit basis. The per unit reactance may be defined as

$$(1.26) \quad X_{p.u.} = \frac{\frac{X}{N^2}}{(\frac{V}{N})(\frac{1}{NI})}$$

where NI is armature rated ampere turns. In order to insure that the mutual reactance is kept the same, we may therefore use equations (1.24) and (1.25) in equation (1.26) to determine rated armature ampere-turns as

$$(1.27) \quad NI \sim K_{Bsat} K_{g}$$

Thus, the power factor scaling constant may be expressed by

$$K_p = K^2_{Bsat} K_g K_\ell K_{a\ell} \quad (1.28)$$

The foregoing discussion describes the modeling procedure. In order to apply the various equations and ratios, slight adjustments are necessary to account for minor variances in the physical, material, and electrical characteristics in the model and generator. These adjustments are demonstrated in Chapter 3.

CHAPTER 2

ELIMINATION OF POLE FACE EDDY CURRENT LOSSES

2.1. Design Modification to Reduce Eddy Current Loss.

The high no-load electrical losses observed in Umans' BIG SANDY model are attributable to pole face eddy current losses.[12] In the model, or any generator for that matter, as the rotor revolves within the stator core, the pole face material is subjected to flux variations caused by the presence of stator slots and teeth. As a result, eddy current pulsations which tend to resist this flux change are induced in the conducting surface of the rotor material.

Pole face eddy current loss in full scale machines is attributed to the fundamental-frequency tooth-ripple flux density, B_t, over the pole and varies as a function of B_t^2.[13] Qualitative insight as to the reasons for the severity of the losses observed in Umans' model is provided by consideration of a family of curves developed by Gibbs,[14] illustrated in figure 2.1, which give the variation of the flux oscillation factor, B_i, as a function of stator slot width to air gap ratio, s/g, and the stator slot width to stator slot pitch ratio, s/λ, for full sized machines. The flux oscillation factor, B_i, is defined as the ratio of fundamental tooth ripple flux density, B_t, previously mentioned, to the average air gap flux density, B_m.

As may be seen from figure 2.1, the model($s/g = 43$, $s/\lambda = .437$) is in a uniquely unfavorable position with regard to high tooth ripple flux density because of the small air gap required to reproduce magnetic diffusion. As a result of this small air gap, however, a simple

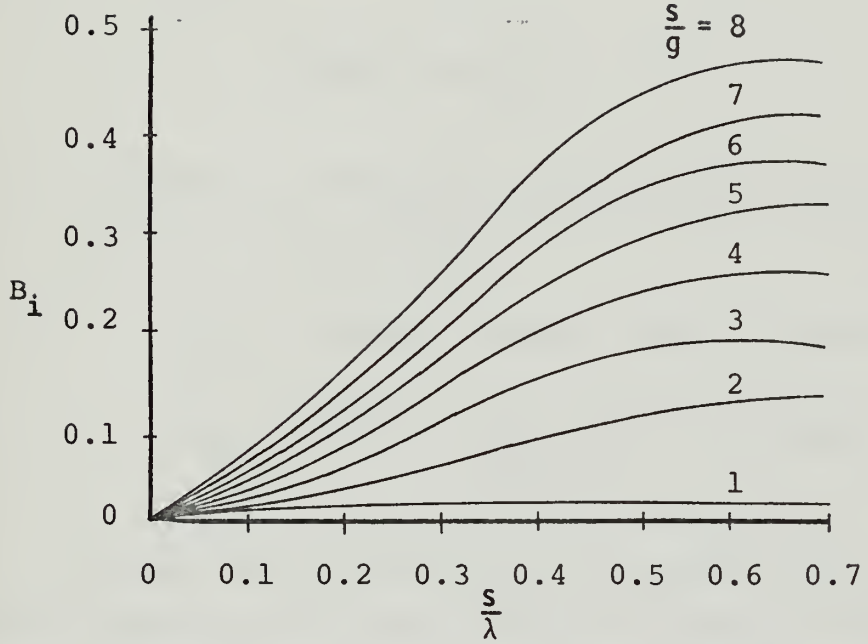

Figure 2.1 Variation of Fundamental Tooth-Ripple Flux Density

approach may be taken to analyze the air gap flux variations in the model.

Consider figure 2.2(b) which is a good approximation for the flux pulsations that would be seen by an observer at point B on the rotor of Umans' model which is illustrated in figure 2.2(a). If we expand the wave form of figure 2.2(b) in a Fourier series, we may determine a frequency spectrum of its harmonic content which is described by[15]

$$(2.1) \quad B_{tn} = \frac{2A}{n\pi} \left| \mathrm{Sin}\left(n\pi \frac{t}{s+t}\right) \right|$$

With the appropriate dimensions substituted into equation (2.1), we obtain the results

$$B_{to} = .4366A = \text{Average value of waveform}$$

$$B_{t1} = .6207A = \text{Amplitude of fundamental harmonic}$$

If we now assume that the average value of the idealized waveform is equal to the average air gap flux density, B_m, we obtain the result that the fundamental tooth ripple flux density at the model pole face is 1.42 B_m which would be expected from figure 2.1.

An analysis by Umans[16] which is based upon this idealized representation of air gap harmonics, indicates that the model eddy current losses are proportional to the square of the harmonic fluxes. His solution is for the power dissipated by a sinusoidal flux wave of known amplitude traveling over a surface of known permeability and conductivity as is illustrated in figure 2.3. The power dissipated is described by

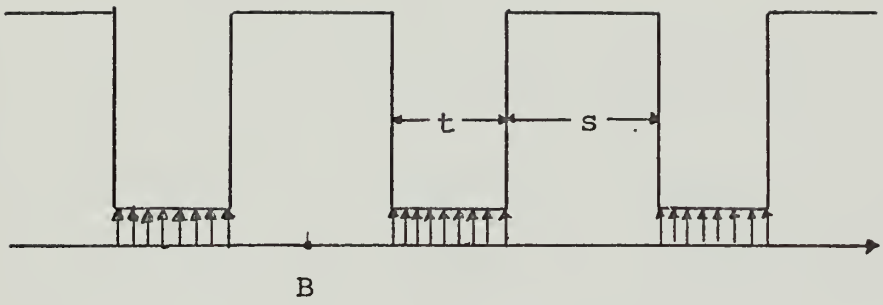

2.2(a) Flux Distribution Over Rotor Pole Face in Umans' BIG SANDY Model

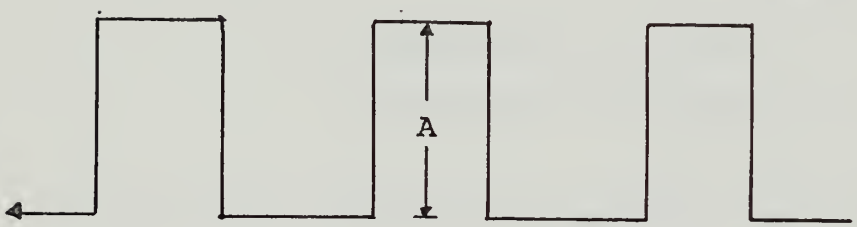

2.2(b) Flux Variations Seen by Observer at Point B

Figure 2.2 Flux Distribution in Umans' BIG SANDY Model

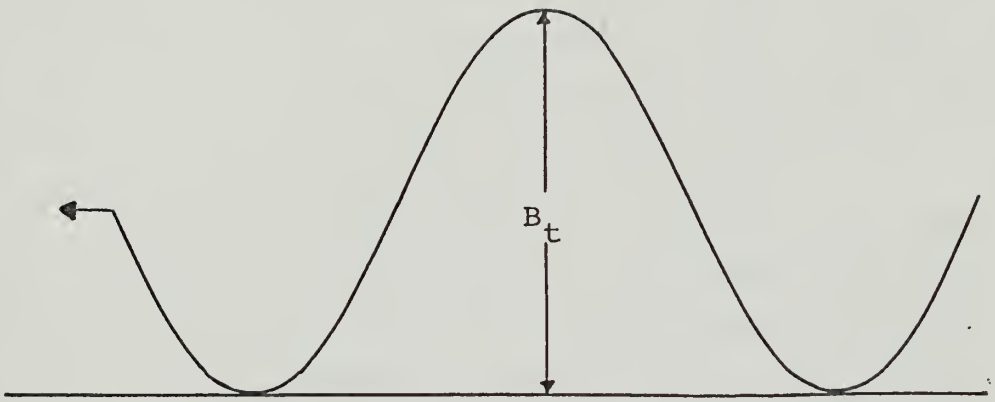

μ = Permeability of Rotor

σ = Conductivity of Rotor

Figure 2.3 Traveling Sinusoidal Flux Wave

$$(2.2)\quad \left\langle \frac{\text{Power Dissipated}}{\text{Area}} \right\rangle = \frac{B_t^2}{8k^2} \sqrt{\frac{2\omega^3\sigma}{\mu}}$$

where B_t = amplitude of flux wave

k = wave number

ω = angular velocity

σ = rotor material conductivity

μ = rotor material permeability

Since the air gap in the model is constrained by the modeling requirement to match magnetic diffusion, the only recourse to reduce the eddy current losses due to tooth-ripple flux is to close the stator slots. This action will in turn produce a secondary effect which is beneficial in that closing the slots will result in a slight increase in the model physical air gap.

In sizing the stator slots for the model, we must consider the relative amplitudes of the higher order harmonics as well as the amplitude of the primary harmonics. Once again, this is because of the fact that the air gap is so small that the power dissipated by these harmonics is not negligible. Table 2.1 illustrates this point. The tabulated values for B_{tn} demonstrate the persistence of the higher order harmonics described by equation (2.1) for the assumed wave form. It must be realized, of course, that the assumption of negligible fringing is less valid as the slot width is reduced. Errors which are included as a result of this assumption are conservative from the viewpoint of reducing the losses.

Before reaching any conclusions from the foregoing analysis, it is necessary to consider another aspect of the eddy current loss phenomena which was unique to Umans' model. As is indicated by equation (2.2), in addition to

being proportional to B_t^2, the eddy current losses are also inversely proportional to $\sqrt{\mu}$.. Because of mechanical problems, it had been necessary to build up the rotor surface of the model with a coating of low permeability iron. Umans calculated that the effect of this iron was to increase the eddy current losses by a factor of 100 over the value predicted by assuming that the design permeability of $47{,}000\mu_o$ was achieved at the rotor surface.[17] The iron was removed by grinding and the losses were reduced by approximately 50%. They were still too high for acceptable operation of the model, however. The fact that the losses remained high may possibly be accounted for by mechanical stresses in the rotor surface due to the grinding operation. A characteristic of the rotor material, demonstrated in tests conducted on material samples by Umans, is that mechanical stress causes a reduction in permeability.[18] The probable need to perform mechanical operations on the rotor dictates that design changes be undertaken to reduce air gap flux harmonics. Because of this and in view of the persistence in amplitude evidenced in the higher order harmonics in table 2.1, it is considered necessary to close the stator slots as much as is practical in order to reduce the eddy current losses to an acceptable level. The value selected for the modified design stator slot width is .040 inch. This decision was reached after consultation with the manufacturer that will provide the stator laminations as being the practical lower limit consistent with lamination cost and die strength.

The loss problem is not completely solved by closing the stator slots, however. It is also necessary to close the rotor slots to prevent similar eddy current losses in the stator while the generator is under load and the

TABLE 2.1

RELATIVE AMPLITUDES OF HARMONICS FOR VARIOUS STATOR SLOT WIDTHS

	S = .2578 in.	S = .050 in.	S = .040 in.
B_{t1}	1.436	.182	.145
B_{t2}	.281	.176	.141
B_{t3}	.401	.166	.135
B_{t4}	.261	.153	.129
B_{t5}	.159	.135	.120

resultant air gap flux is at some angle with the direct-axis. The slot width for the modified rotor design is .050 inch. This value was chosen to facilitate hand winding of the rotor. As is indicated in table 2.1 by the tabulated values of B_{tn} for a .050 inch slot width, this choice should not result in a large increase in the eddy current loss with the machine operating under loaded conditions.

2.2. Experimental Verification of Loss Reduction Method.

An experiment was conducted to verify that closing the stator slots would reduce the no-load losses. This experiment consisted of inserting steel bars into the slots of Umans' BIG SANDY model to simulate a closed slot structure. It was conducted before the low permeability iron material was ground off the surface of the rotor.

The test procedure was to drive the model generator with a d.c. motor at a constant angular velocity of 3600 r.p.m. with the generator terminals open. The generator field current was increased from 0 amperes to the value determined necessary to give rated voltage for the open slot configuration of 1.2 amperes. The d.c. motor was operated with the field separately excited. Adjustments in power necessary to maintain a constant speed of 3600 r.p.m. were applied by means of a variable resistor connected in series in the motor armature circuit. Measurements of the motor armature voltage and current were recorded for the various levels of excitation of the generator. The electrical power dissipated by the generator was determined at any particular level by taking the difference between the observed power supplied to the d.c. drive motor for that level and the amount that was supplied with the

generator unexcited. Coincidentally, a measurement of the air gap flux level in the generator was taken by integrating the voltage output of a one-turn coil, short-pitched two slots, which was inserted in the generator stator.

Three experiments using this procedure were conducted with the steel bars in the slots. The resultant modified slot configuration is illustrated in figure 2.3. The bars were then removed, and two experiments were conducted following the same procedure.

The results of these tests, averaged for each slot configuration, are presented in figures 2.4 and 2.5. As is indicated in figure 2.4, a reduction of approximately 20% in electrical losses was observed with the bars inserted in the slots. We may consider qualitatively the significance of this result as an indication that closing the slots in the modified design will reduce these losses to an acceptable level by interpreting the flux measurements depicted in figure 2.5.

As is illustrated, there was an increase in flux of approximately 5% observed for the same excitation with the bars in the slots. Since the physical air gap was the same for both experiments, this indicates that the presence of the bars caused an equal reduction of 5% in the model's effective air gap. If the slots were closed by the same amount by means of tooth extensions at the air gap interface, the physical gap of the model would approximately equal the effective or electrical gap. The effective air gap for Umans' model is .013 inch[19] and the physical gap, as indicated, is .006 inch which suggests that we would expect to see an increase in flux of approximately 50% for the same excitation if the slots were

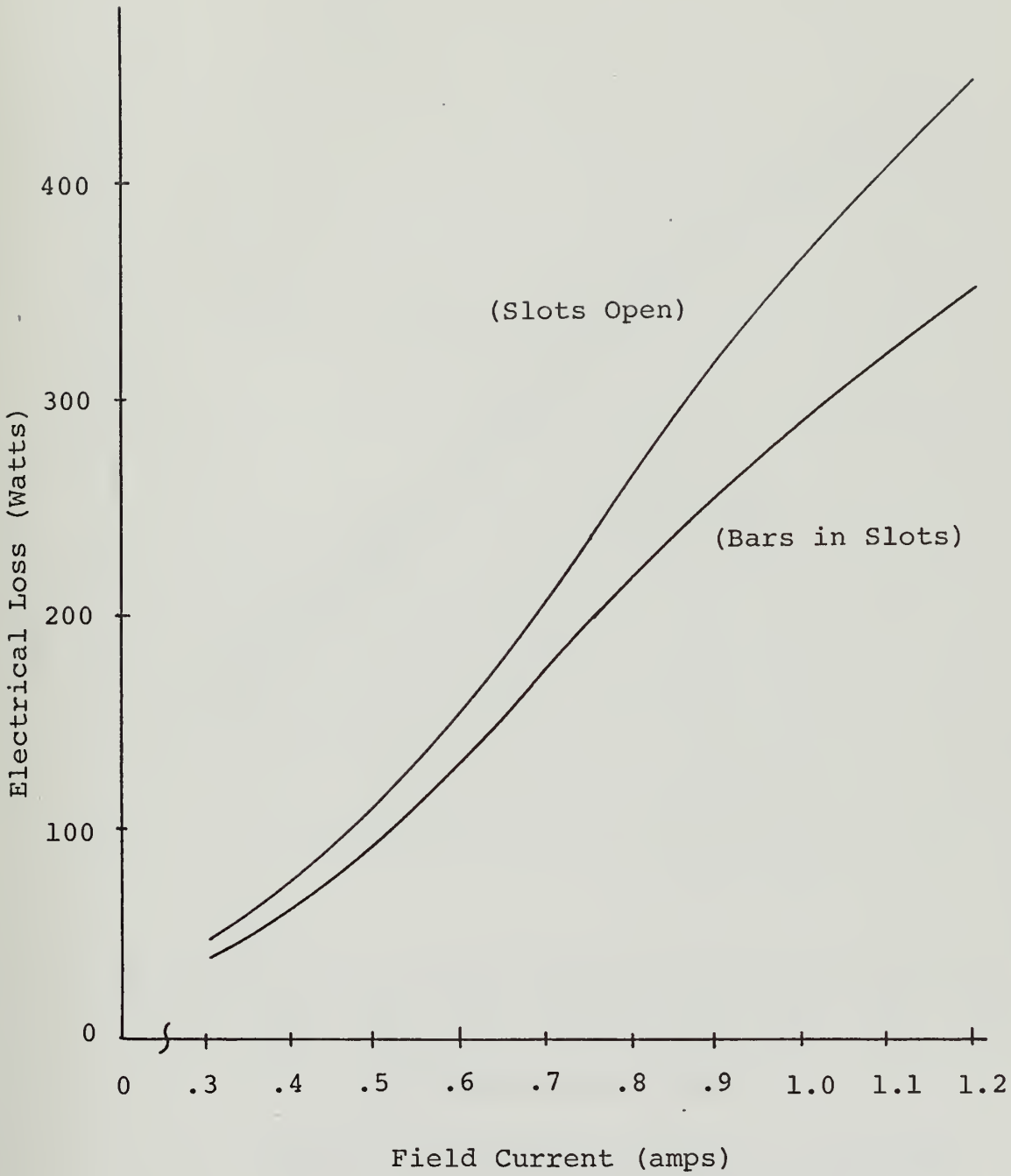

Figure 2.4 No-Load Electrical Loss Test
Loss Measurements

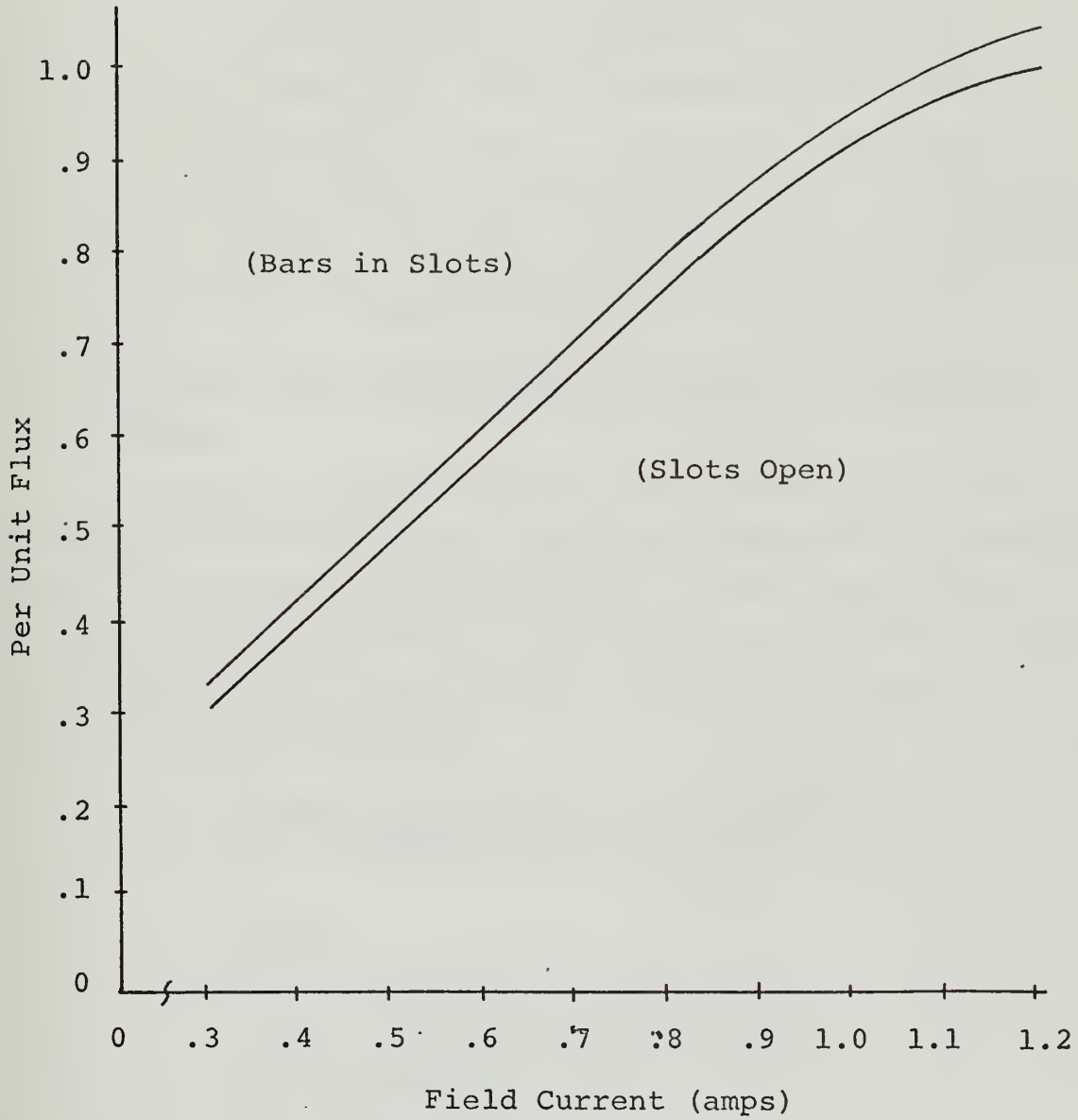

Figure 2.5 No-Load Electrical Loss Test
Flux Measurements

effectively closed at the air gap interface for the same physical gap.

The small increases in flux due to the presence of the bars thus indicates that the effectiveness of the bars in the slots, as far as simulating a closed slot configuration, was poor. This is understandable since aligning and securing the bars in the slots was a most difficult task. The fact that a 20% reduction in electrical losses occurred with bars indicates that to effectively close the slots would substantially reduce the losses as is predicted by the theory developed in section 2.1.

2.3. No Load Eddy Current Loss Calculation for Modified Design.

In order to apply equation (2.2) to calculate the no-load loss due to the air gap space harmonics, we assume linear superposition and calculate the loss contribution for each harmonic component, then sum the resultant losses to determine the no-load losses. This may be expressed mathematically as follows:

$$(2.3) \quad \left\langle \frac{\text{Power Dissipated}}{\text{Area}} \right\rangle = \sum_{n=1}^{\infty} \frac{B_{tn}^2}{8k_n^2} \sqrt{\frac{2\omega_n^3 \sigma}{\mu}}$$

where

B_{tn} = amplitude of nth harmonic

$\omega_n = 24n\omega_o$

$k_n = \frac{24n}{r}$

σ = conductivity of rotor material

μ = permeability of rotor surface

in order to account for the fact that a point on the rotor passes under 24 stator slots in one complete revolution.

The average value to use in determining the amplitude of the losses over the pole face is the peak value of the fundamental air gap flux wave described by[20]

$$(2.4) \quad B_p = \frac{P}{2} \frac{E_{Rms}}{(2lr)(4.44fk_wN_{ph})}$$

$E_{Rms} = R_{ms}$ volts per phase

f = frequency

k_w = winding reduction factor

N_{ph} = series turns per phase

l = machine active length

r = rotor radius

Additionally, if we assume a sinusoidal distribution for the fundamental flux as illustrated in figure 2.6, the contribution to the losses due to the teeth adjacent to the pole face may be determined by the relation

$$(2.5) \quad \left\langle \frac{\text{Power Dissipated by Tooth}}{\text{Area}} \right\rangle = \left\langle \frac{\text{Power Dissipated by Pole Face}}{\text{Area}} \right\rangle \times \left(\frac{B_{ho} \text{ for Pole Face}}{B_{ho} \text{ for Appropriate Tooth}} \right)^2$$

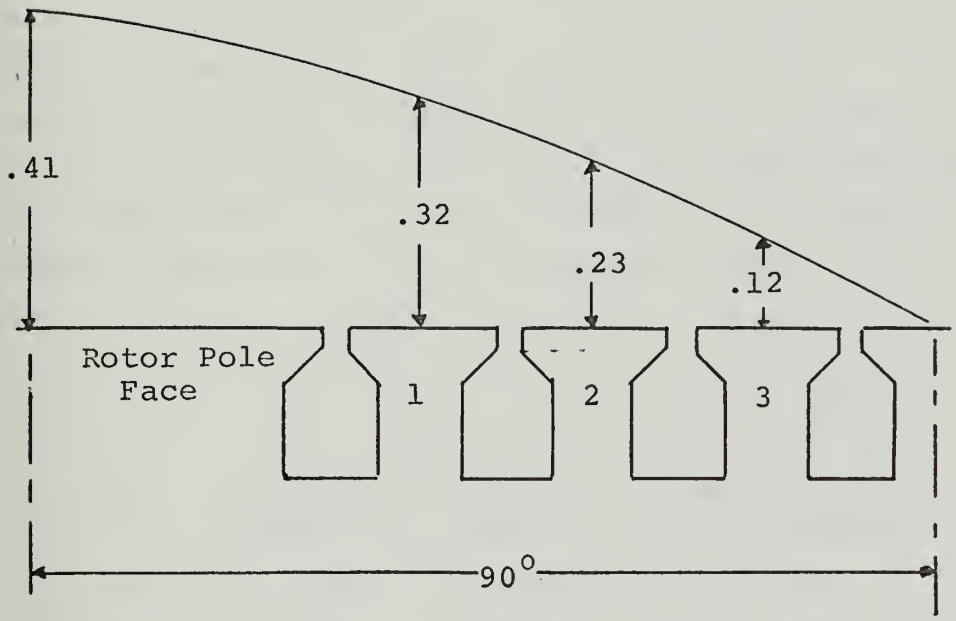

Figure 2.6 Air Gap Flux(webers/meter^2) Values Assumed for Loss Calculation

The value chosen for the permeability of the rotor material in this calculation is $2{,}000\mu_o$. This value was chosen based upon the results of Umans' observation of the reduction in losses when the lower permeability iron was removed from the rotor.[21] The actual value of permeability for the iron covered rotor was approximately 1/100 the assumed value for the rotor surface which was $47{,}000\mu_o$. The observed reduction in losses when the iron was removed was approximately 50% or 1/2 which indicates that the surface permeability of the rotor in its final configuration was increased by a factor of 4 to approximately $2{,}000\mu_o$.

From equation (2.4), $B_{to} = .41$, using equation (2.3), the loss contribution due to each of the first five harmonic components of the air gap flux over the pole face is

n	B_{tn}	k (Meter^{-1})	ω_n (Sec^{-1})	$\frac{B_{tn}^2}{8k_n^2}\sqrt{\frac{2\omega_n^3\sigma}{\mu}}$ (Watts/Meter^2)
1	.060	420	9,050	87
2	.057	840	18,100	55
3	.055	1,260	27,100	46
4	.052	1,680	36,200	38
5	.049	2,100	45,200	26

Thus, the total power dissipated per unit area over the pole face is 247 watts/meter^2. The total pole face area for the rotor is .025 square meters. Consequently, the eddy current loss is approximately 6 watts.

The power dissipated per tooth is, by equation (2.5),

Tooth	B_{ho} Tooth	$\left(\frac{B_{ho}\text{ Tooth}}{B_{ho}\text{ Pole Face}}\right)^2$	$\left\langle \frac{\text{Power Dissipated by Tooth}}{\text{Area}} \right\rangle$ (watts/meter)
1	.32	.61	150
2	.23	.31	77
3	.12	.086	21

The terms, tooth 1, tooth 2, tooth 3, correspond to the tooth location illustrated in figure 2.6.

There are four teeth at each location (1,2,or 3) and each tooth has the same area of .0028 square meters, then

$$\left\langle \text{Power Dissipated by Rotor Teeth} \right\rangle = 4 \times \sum_{n=1}^{3} \left\langle \frac{\text{Power Dissipated by Tooth n}}{\text{Area}} \right\rangle$$

$$\times .0028 = 4 \times (248) \times .0028 = 3 \text{ watts}$$

Thus, the total no-load eddy current loss predicted for the modified design is approximately 9 watts.

CHAPTER 3

MODIFIED DESIGN

3.1. General.

The stated object of this thesis is to provide a modified model design so as to eliminate the no-load electrical loss problem and provide rotor and stator laminations which are suitable for use in models of other AEP generators than BIG SANDY. The loss problem was addressed in Chapter 2; in this Chapter, the rotor and stator laminations are designed to be suitable for models of either BIG SANDY No. 2 or MITCHEL No. 1 generating units. By providing laminations suitable for models of these generators, we should achieve the second stated objective in that these units represent the extremes of the generators to be modeled. BIG SANDY and MITCHEL have respectively the smallest air gap with the shortest active length and the longest air gap with the smallest active length of the machines to be modeled.

3.2. Experimental Prediction of K_{Bsat}.

It is important to be able to predict the value of K_{Bsat} which will be achieved in the model design since this constant affects nearly all aspects of the design. The failure to accurately determine K_{Bsat} for Umans' BIG SANDY model resulted in the stator slots being too small to accommodate the number of turns required to achieve the designated rated voltage. The calculated value of K_{Bsat} was .4, and the actual value determined by Umans was .32.[22]

The method used to calculate K_{Bsat} for Umans' model was proposed by Haller.[23] Haller reasoned that saturation

would occur at the base of the pole in the model as it does in the actual generator. Additionally, he concluded that saturation would occur sooner in the model because of the reduced cross-sectional area in the pole face due to the holes for the copper rods. His procedure to express the resultant reduced saturation level was to take a ratio of the total arc length across the pole face at the radius of the rods, less the length eliminated by the holes, to the total arc. This ratio was multiplied by another ratio which compared the relative saturation characteristics of the material used in the model lamination to that for the BIG SANDY rotor iron to obtain K_{Bsat}, i.e.,

$$K_{Bsat} = \frac{B_{sat\ eff}}{B_{sat\ mat}} \times \frac{B_{sat\ 4750}}{B_{sat\ BIG\ SANDY}}$$

The disparity between the predicted and measured values for K_{Bsat} of Umans' model indicate that saturation occurs at some point other than at the base of the pole face. Because of the numerous holes in the rotor lamination, there are an infinite number of cross-sections at which saturation might occur. A teledeltos model may be used to understand more fully the effects of these holes in the rotor lamination on the rotor flux.

Figure 3.1 illustrates the teledeltos modeling technique. The current measured between equipotential surfaces, represented by silver paint, on the direct or quadrature-axis is analogous to the flux which flows between these surfaces in the actual rotor. The changes in current which are observed due to the addition of holes in the teledeltos paper, which correspond to the holes in

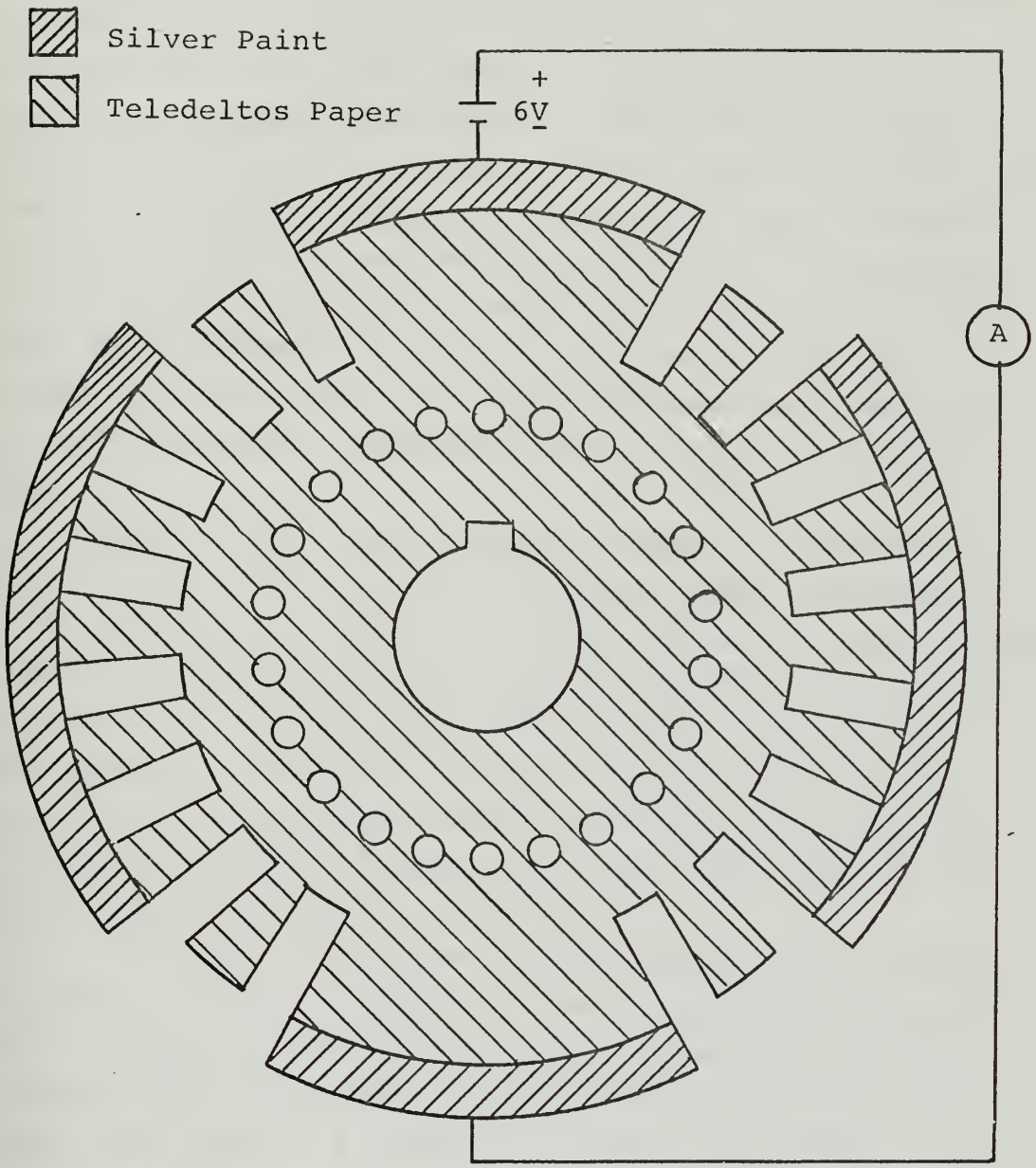

Figure 3.1 Teledeltos Model

the rotor laminations, are thus analogous to the changes in reluctance in the rotor laminations. Since teledeltos paper is a linear device, the model affords no exact way to measure saturation. The measured changes in reluctance due to the holes tend to correlate with the observed changes in saturation in Umans' model, however. If, for instance, we assume that the drop in reluctance is a measure of the drop in saturation level due to the holes in the rotor and combine this result with the changes in saturation due to the differences in material, the model predicts a value of .32 for K_{Bsat} for Umans' model.

Qualitatively, the measured change in reluctance using the teledeltos model should give some indication of the expected reduction in saturation in the model rotor since the distortion of the linear B-field in the rotor by the holes is reflected in the relative reluctance measurements. The holes located near the base of the pole face, for instance, cause a greater drop in the reluctance of the path between the pole faces than do the holes near the center of the rotor.

If in fact the change in reluctance is any measure of saturation characteristics, the teledeltos model predicts a K_{Bsat} of .38 for the modified lamination design. In other words, the distribution of holes in the rotor caused much less of a reduction in the reluctance of the path between the pole faces in the modified rotor design than did the holes in Umans' rotor. The location of holes in the rotor pole face is the same for both designs. Based upon these facts, a value for K_{Bsat} of .36 is chosen for the modified design. This is conservative from the point of view of the teledeltos test results. Additionally,

the stator slot size required to accommodate the number of turns to generate designed rated voltage as a result of this choice, approaches the practical limit. If K_{Bsat} turns out to be smaller, a lower rated voltage will have to be accepted.

One additional benefit was derived from the teledeltos tests. The tests conducted on Umans' rotor design indicated that the relative reluctance changes were different along the direct and quadrature-axis because of the holes added to the pole face of the rotor. This condition is undesirable in the model because it would result in the model exhibiting a salient effect which does not occur in the full sized generator. It was found using the teledeltos analog that this problem could be resolved by the addition of holes in the rotor teeth; consequently, these holes are included in the modified lamination design.

3.3. Modified Design.

The purpose of this section is to delineate the design judgments which effected the choice of model parameters to accomplish the stated objectives. The modified design procedure developed by Umans is followed; the numerical computations up through and including the calculation of the area of copper necessary to model the field discharge time constant were accomplished with the use of Umans' model design program.[24] The applicable design equations from section 1.3 are listed and re-numbered in table 3.1. The various scaling parameters discussed in the following paragraphs are tabulated in table 3.2. The physical and electrical descriptions of the full scale generators are listed in tables 3.3 (BIG SANDY) and 3.4 (MITCHEL I) along with a description of the appropriate

TABLE 3.1

SCALING CONSTANT RELATIONS

$$K_v = K_n \frac{K_{Bsat} K_\ell^2 K_{a\ell}}{K_t} \qquad (3.1)$$

$$K_i = \frac{K_{Bsat} K_g}{K_n} \qquad (3.2)$$

$$K_p = \frac{K_{Bsat}^2 K_\ell^2 K_g K_{a\ell}}{K_t} \qquad (3.3)$$

$$K_\mu K_\sigma K_\ell^2 = K_t \qquad (3.4)$$

$$\frac{K_\mu K_g}{K_\ell} = 1 \text{ (From } \underline{C} \text{ Constant)} \qquad (3.5)$$

TABLE 3.2

MODEL CONSTANT VALUES

	BIG SANDY	MITCHEL
K_t	1.0	1.0
K_p	10^{-6}	10^{-6}
K_ℓ	.1	.1
K_σ	2.9985	2.1739
K_μ	32.61	42.00
μ_{mat}	$45{,}800\mu_o$	$58{,}990\mu_o$
K_g	.0031	.0025
$K_{a\ell}$	.243	.283
K_v	.0088	.0088
K_n	9.87	10.58
AROD	.0513 $in.^2$	.0570 $in.^2$
ARODT	.0010 $in.^2$	.0012 $in.^2$

model design. Figure 3.2 illustrates the new rotor lamination design and figure 3.3, the new stator lamination design.

The time, K_t, power, K_p, and length, K_ℓ, scaling constants are chosen to yield a model which is of convenient size for laboratory use and reasonably inexpensive to produce. The selected values, table 3.2, as demonstrated by Umans' model, fulfill these requirements.

The copper fraction, f_c, is defined as the ratio of the area of copper to the total area of the rotor lamination excluding the areas of slots and shaft. In order to use the same laminations for both models, it is necessary to use different copper fractions. The primary reason for this, as will be seen later, is to restrict the amount of copper in the rotor slots which must be added to match the field discharge time constant. The particular copper fractions used in the modified design are selected to achieve a balance among model physical air gap length, active length, and rotor slot dimensions. The distribution of copper within the rotor is made uniform so that the rotor will appear as homogeneous as possible to transverse fields. The conductivity scaling constant, K_σ, is fixed by the choice of f_c.

We now may determine the permeability scaling constant, K_μ, from equation (3.4)

$$(3.6) \quad K_\mu = \frac{K_t}{K_\sigma K_\ell^2} .$$

The effective permeability is computed from the definition of K_μ.

$$(3.7) \quad \mu_{eff} = K_{\mu}\mu_{generator}$$

The permeability which must be achieved in the rotor material is slightly higher than μ_{eff} because of the holes in the rotor lamination. This value is calculated from the empirical formula.[25]

$$(3.8) \quad \mu_{eff} = (.9-1.29f_h)\mu_{mat}$$

where f_h is the hole fraction in the rotor lamination. The definition for f_h is similar to that for f_c. The permeability requirements obtained for both BIG SANDY and MITCHEL 1 are achievable with the use of 4750 material from Allegheny-Ludlum, the material used in Umans' model.

The air gap scaling constant is now defined by equation (3.5).

$$(3.9) \quad K_g = \frac{K_{\ell}}{K_{\mu}}$$

A distinct advantage in closing the rotor and stator slots to reduce the eddy current losses is realized in the model physical air gap. The effects of both rotor and stator slots are negligible, and the physical air gap equals the effective air gap.

The model active length (MAL) is scaled from the generator active length (GAL) using equation (3.3) as follows:

$$(3.10) \quad K_{a\ell} = \frac{K_p K_t}{K_{Bsat}^2 K_{\ell}^2 K_g}$$

$$(3.11) \quad MAL = K_{a\ell} K_{\ell} GAL$$

Next, we calculate the field ampere-turns necessary for rated voltage using equation (3.3).

$$(3.12) \quad (N_f I_f)\text{Model} = K_g K_{Bsat} (N_f I_f)\text{Generator}$$

The model armature series-turns per phase (NAM) required for 230 $\text{volts}_{\ell\text{-}\ell}$ is determined from the generator series-turns per phase (GNAM) using equation (3.1).

$$(3.13) \quad K_n = \frac{K_v K_t}{K_{Bsat} K_{\ell 2} K_{a\ell}}$$

and

$$(3.14) \quad \text{NAM} = K_n \times \text{GNAM}$$

Finally, we calculate the cross-sectional area of copper necessary in the top (ARODT) and bottom (AROD) of the rotor slots to match the initial generator sub-transient and field discharge time constants. Tests conducted by Haller on the CARDINAL model demonstrated the need for the inclusion of copper in the outer extremity of the rotor to correctly model these effects. His solution to the problem was to calculate the radius of rods arranged in cylindrical rows in the bottom and top of the rotor slots respectively, that would have the appropriate discharge time constant.[26]

$$(3.15) \quad r_{rod} = \frac{2\tau}{\mu_o \sigma} \frac{1}{N} \left(\frac{R_a^2 - R_f^2}{R_a^2 + R_f^2} \right)$$

where σ = conductivity of rod

N = number of slots

r_{rod} = radius of rods

R_f = rotor radius to middle of rods

R_a = R_f plus air gap length

A rectangular shape is more useful in the rotor slots; consequently, copper bars with cross-sectional areas equivalent to the rods are used in the modified design.

As was previously mentioned, the requirement to include this copper in the rotor slots imposes a constraint on the copper fraction for the rotor bulk (f_c) in that AROD is proportional to the air gap length which is in turn inversely proportional to the rotor copper fraction (f_c). The rotor copper fraction is thus limited by the rotor slot size.

Figures 3.2 and 3.3 illustrate the new rotor and stator laminations. The basic difference between these laminations and those used in Umans' design are in the distribution of copper in the rotor and in the slot configurations. Since the number and location of slots are kept the same, the field and armature turns distribution designed for Umans' model may be used.[27]

The field winding will be distributed in four coils per pole with 32 turns per slot except for the four slots adjacent to the pole face which will contain 28 turns. However, the field is to be wound from No. 18 wire which is larger than that used by Umans. Identical field windings are to be used for both the BIG SANDY and MITCHEL 1 models; thus, the MITCHEL 1 model will operate at slightly higher field current levels.

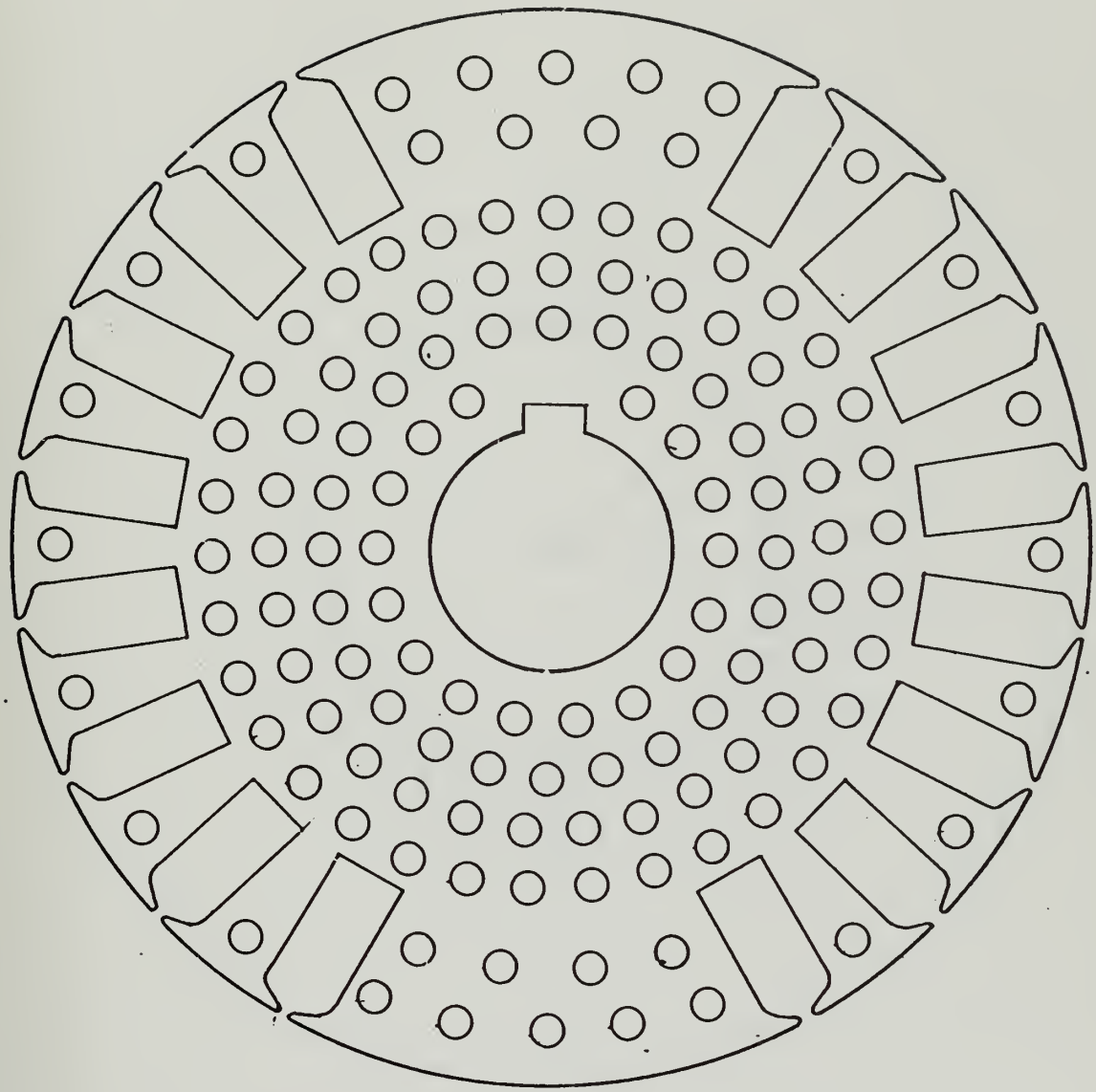

Figure 3.2 Modified Rotor Lamination

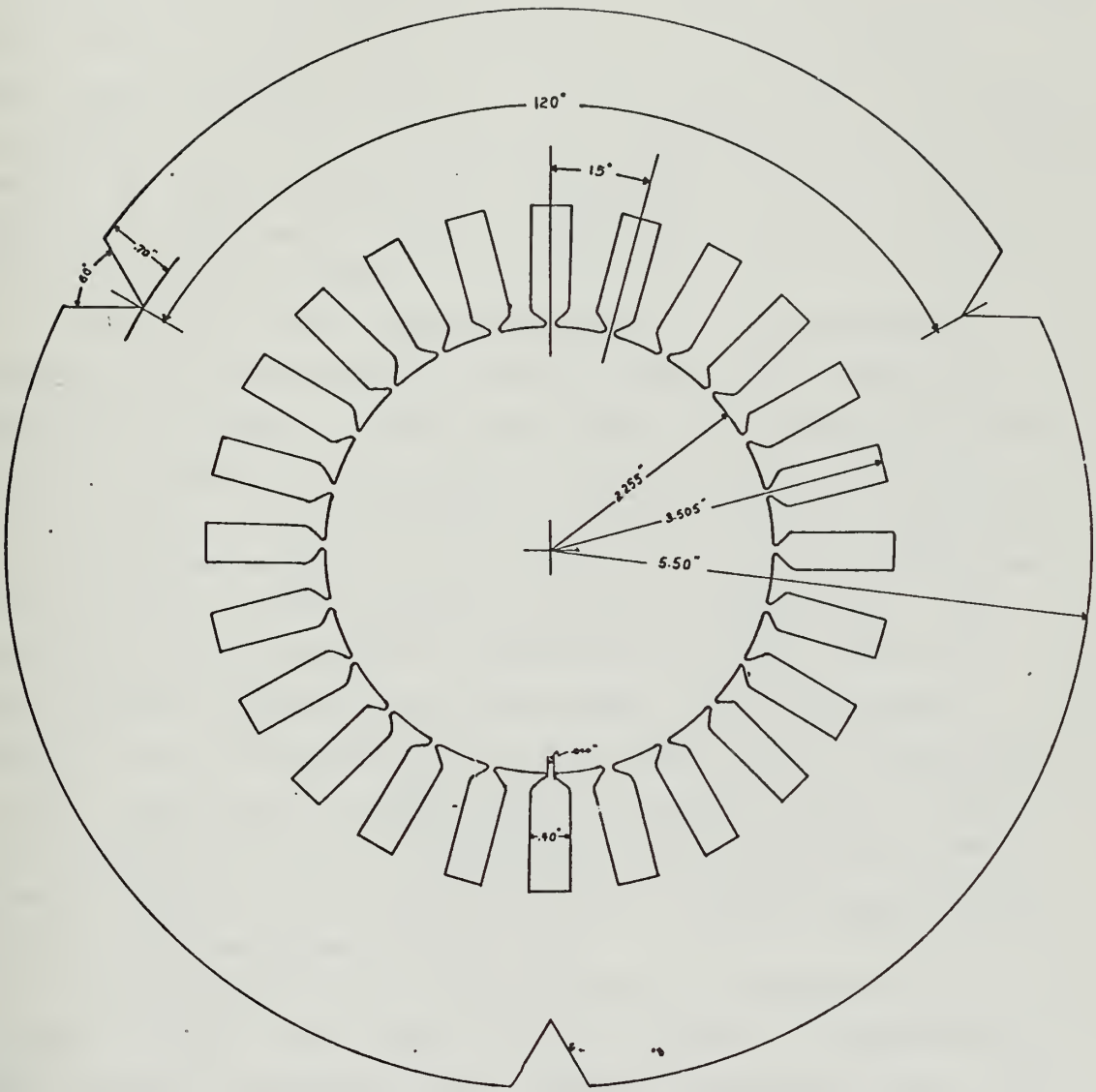

Figure 3.3 Modified Stator Lamination

The armature winding will have 4 coils in series per phase with two parallel paths. The winding will be short pitched 2 slots and distributed in 6 slots. The required turns per armature slot for each design to achieve 230 volts$_{\ell-\ell}$ is 30 for BIG SANDY and 32 for MITCHEL 1. The required packing factor for both the rotor and stator windings is .5. The rotor field resistance will be approximately 5Ω and the armature resistance will be .127Ω per phase or .0022 p.u. for BIG SANDY and .135Ω per phase or .0023 p.u. for MITCHEL 1.

The rotor slot configurations for the MITCHEL 1 design is illustrated in figure 3.4(a). The slot is sized for MITCHEL 1 since more copper is required in the slot. In addition to designing the slot so that it is large enough to accommodate the field windings and AROD, it is also necessary to insure that the tooth extensions which close the slot do not saturate prematurely. The extensions are designed, therefore, so that they will not saturate before the tooth shank. Note also that ARODT is not included in the rotor slot but in the holes in the rotor teeth illustrated in figure 3.4(b). This arrangement is one of convenience since holes must be located in the rotor tooth tops to balance K_{Bsat} on the direct-axis and quadrature-axis.

The stator slot configuration is illustrated in figure 3.5(a). The stator slot is sized to accommodate the MITCHEL 1 winding which contains the most turns. The extensions for the stator teeth, shown in figure 3.5(b), also are designed so that they will not saturate before the shank portion of the tooth. The stator slot width design is influenced by the need to insure that the stator teeth saturate simultaneously with the occurrence of

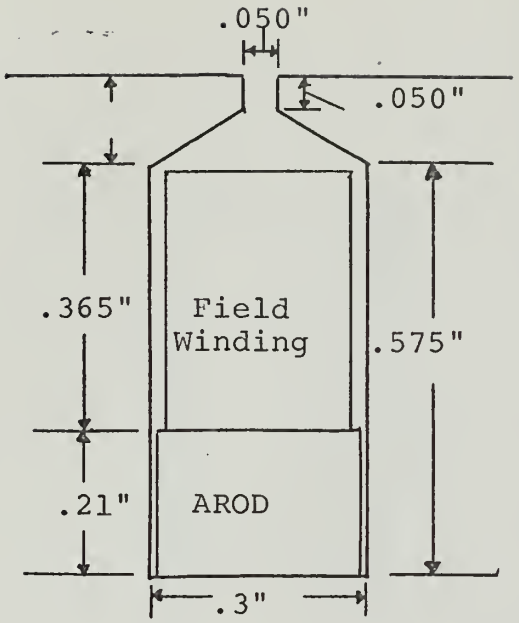

(a) Rotor Slot

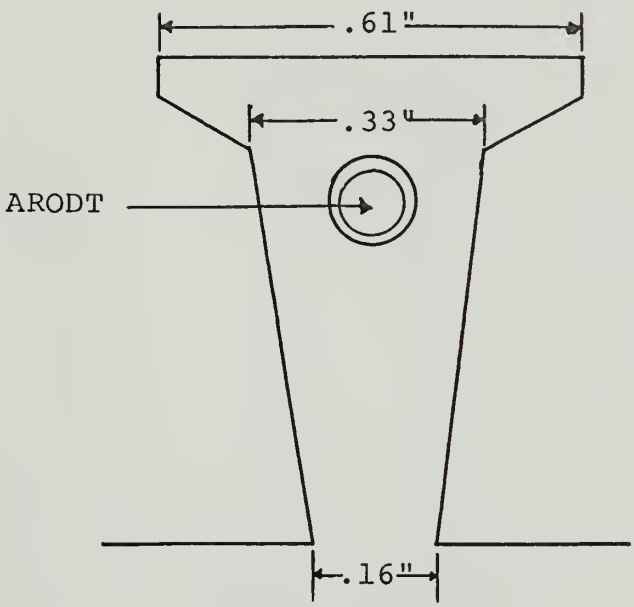

(b) Rotor Tooth

Figure 3.4 Modified Rotor Tooth and Slot Configurations

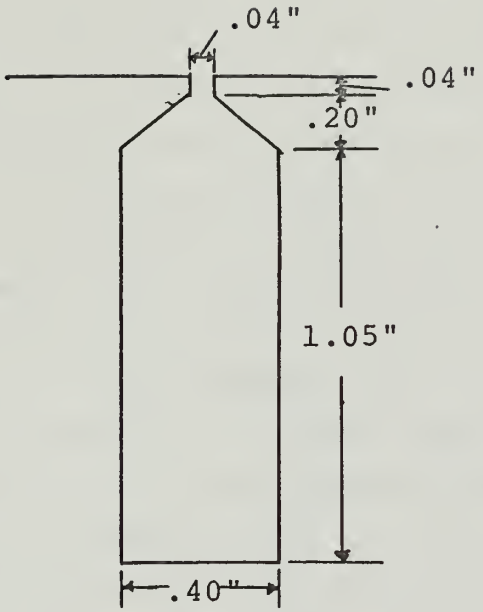

(a) Stator Slot

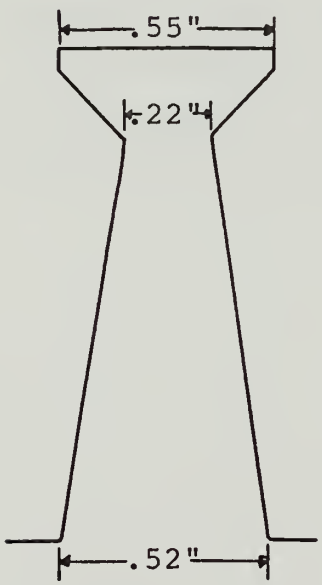

(b) Stator Tooth

Figure 3.5 Modified Stator Tooth and Slot Configurations

saturation in the rotor, as is the case in an actual generator. This may be accomplished by reducing the stator tooth width to stator slot pitch ratio by an amount equal to the reduction in the saturation level in the rotor that is caused by the holes in the rotor laminations. A second technique which may be employed is the reduction of the stator core area by including toothless stator laminations in the stator stack.[28]

The teledeltos model tests described earlier indicate that the rotor saturation flux level is reduced by 40% for the modified rotor lamination. In order to match this in the stator for the BIG SANDY and MITCHEL 1 designs, a combination of the procedures described above are used. The stator tooth width to slot pitch for the full scale machines are .563 and .497 for BIG SANDY and MITCHEL 1 respectively. The modified model stator tooth width to tooth pitch ratio at the most narrow portion of the tooth is .377. The desired ratio for the BIG SANDY model is .34 which indicates that 10% toothless laminations should be included in the stator stack to exactly model saturation. For the MITCHEL 1 design, the desired tooth width to slot pitch ratio is .298 which indicates that 20% toothless laminations should be included in the stack.

TABLE 3.3

	BIG SANDY	MODEL
Fraction of Copper	--	.200
Effective Conductivity	$.067\sigma_c$	$.200\sigma_c$
Rotor Permeability	$860\mu_o$	$45{,}800\mu_o$
Air Gap Length	2.875 inches	.009 inches
Effective Air Gap Length	2.875 inches	.089 inches
Rotor Radius	22.25 inches	2.25 inches
Field Winding Turns	92	248
Rotor Field Current	5294 amps	2.2 amps
Armature turns in Series per phase	6	60
Rated Armature Voltage ℓ-ℓ	26,000 volts	230 volts
Power Rating	907 MVA	907 VA

TABLE 3.4

	MITCHEL I	MODEL
Fraction of Copper	--	.145
Effective Conductivity	$.061\sigma_c$	$.145\sigma_c$
Rotor Permeability	$860\mu_o$	$58,990\mu_o$
Air Gap Length	4.3 inches	.011 inches
Effective Air Gap Length	4.3 inches	.0107 inches
Rotor Radius	21.5 inches	2.25 inches
Field Winding Turns	124	248
Rated Field Current	6075 amps	2.7 amps
Armature turns in Series per phase	8	64
Rated Armature Voltage ℓ-ℓ	26,000 volts	230 volts
Power Rating	907 MVA	907 VA

CHAPTER 4

LEAKAGE REACTANCES

4.1. General

It has been assumed in the design of past physical scale models that the model leakage reactances would be relatively smaller than those observed in the full size generators because of the model's relatively smaller air gap.[29] This assumption has been proved valid by tests conducted on the CARDINAL and Umans' BIG SANDY models.[30] It is deemed necessary to calculate the leakage reactances for the modified design which is the subject of this Chapter, first of all to insure that the leakages will continue to be small and thus correctable, and secondly, to calculate if possible, the values of external reactance necessary in the field and armature circuits of the model to match the direct-axis transient and synchronous reactances of the full scale generator.

4.2. Armature Leakage Reactance.

Armature leakage reactance may be described as the difference between the total flux produced by the armature current alone and the space fundamental of the flux in the air gap. It is composed of four parts due to the following reactances.[31]

(a) slot leakage reactance
(b) coil end leakage reactance
(c) tooth-top leakage reactance
(d) differential leakage reactance

The magnetic paths for the leakage flux which create the above defined leakage reactances are illustrated in figure 4.1. By the principle of linear superposition, we

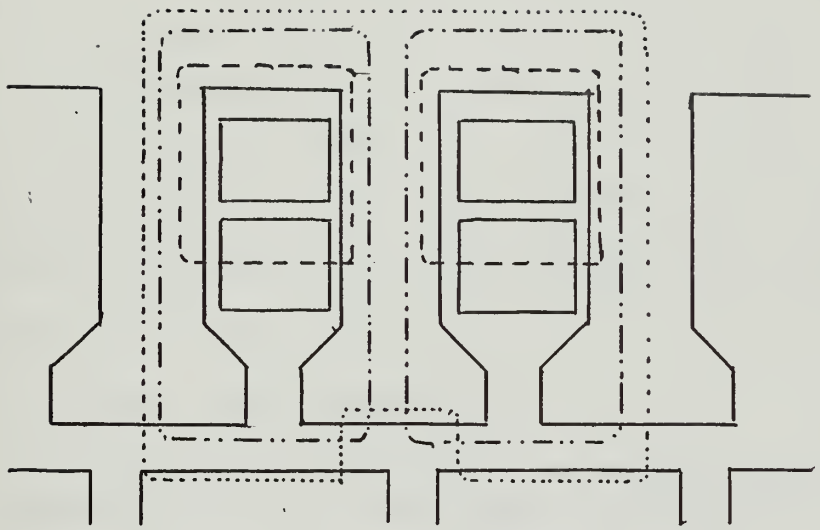

– – – – = Slot Leakage
—··—··- = Tooth-Top Leakage
····· = Differential Harmonic Leakage

Figure 4.1 Magnetic Paths for Armature Leakage Fluxes

may calculate separately the leakage reactance due to each one of these components, and then sum the results to obtain the total leakage reactance.

4.2.a. Tooth-Top Leakage (X_{at})

The tooth-top leakage reactance is, as illustrated in figure 4.1, due to leakage fluxes which lie in the air gap and cross from tooth-top to tooth-top. The value of this component may be determined from curves provided in a paper by M. E. Talaat.[32] Talaat's results were obtained from application of the Schwarz-Christoffel transformation to the slot air gap configuration. Tooth-top leakage is negligible in the physical scale models because of the small air gap.

4.2.b. Stator-Slot Leakage (X_{as})

The following procedure to calculate the model stator slot leakage is from a development by Alger.[33] The stator slot leakage is equal to the product

(4.1) ω x slots per phase
x (series conductors per slot)^2
x embedded length of slot
x slot permeance ratio x μ_o

or

$$(4.2) \quad X_{as} = \omega\left(\frac{S}{q}\right)\left(\frac{2qN}{S}\right)^2 (L)(P_s)\mu_o$$

$$= \omega q L (N)^2 (P_s)\mu_o \text{ ohms per phase}$$

where s = number of stator slots
q = number of phases
N = armature series-turns per phase
L = machine active length

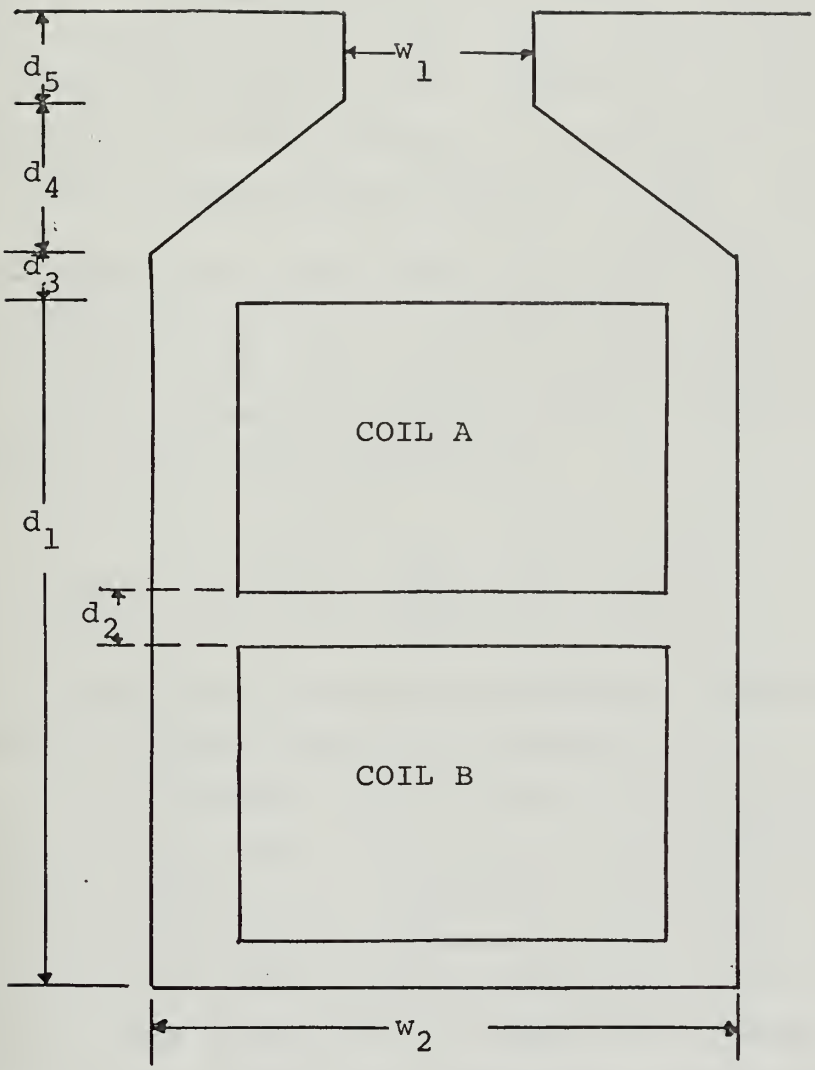

Figure 4.2 Slot Dimensions for Leakage Calculation

The slot permeance ratio, P_s, may be determined by considering the slot flux linkages for the slot configuration in figure 4.2. The linkages are composed of four parts which must be summed to give the total flux linkages. The flux crossing the opening and linking all the conductors is expressed by the ratio of depth to width of slot opening, d_5/w_1. The flux crossing the neck of the slot also links all the conductors in the slot; it is measured by the integral of the depth over width ratio and is approximately equal to $\frac{2d_4}{w_2+w_1}$. The flux crossing the slot above the top of the coil, linking all the conductors in the slot equals d_3/w_2. Finally, the flux crossing the body of the slot and linking only a part of the conductors equals $d_1/3w_2$. The resultant expression for slot permeance is

$$(4.3) \quad P_s = \frac{d_5}{w_1} + \frac{2d_4}{w_1+w_2} + \frac{d_3}{w_2} + \frac{d_1}{3w_2}$$

and is valid for a full pitch winding in which both coils in the slot carry identical currents.

If the winding is fractional pitched, the currents in the coils in some slots are out of phase by an electrical phase angle θ. In a balanced fractional pitched winding, the out-of-phase components will cancel since there are an equal number of slots containing lower coil sides which lag the upper coil's current by an angle θ as there are slots with upper coil sides with currents which lead by the same angle θ. These out-of-phase components will cancel and we need only consider the in-phase components of induced voltage. The mutual inductance between coils carrying currents θ^{o} out-of-phase must be multiplied by

$\cos\theta$ to determine the effective mutual inductance.

The total slot reactance may be expressed as (refer to figure 4.2)

$$(4.3) \quad X = X_A + 2X_{AB} + X_B.$$

Now, for a straight slot of width, w_2, the slot permeance ratio for conductor A is

$$(4.4) \quad P_A = \frac{d_3}{w_2} + \frac{d_1-d_2}{6w_2}$$

The expression for mutual permeance between A and B is

$$(4.5) \quad P_{AB} = \left(\frac{d_3}{w_2} + \frac{d_1-d_2}{4w_2}\right) \cos\theta$$

The current in B produces a uniform flux density crossing the slot over the height of A. The voltage induced in A by this flux density varies linearly from top to bottom of A and is equivalent to one-half of the flux in B linking all of A. Thus, one-half the height of A or $(d_1 - d_2)/4$ is effective in producing mutual inductance.

The slot permeance ratio for B is

$$(4.6) \quad P_B = \frac{d_3}{w_2} + \frac{4(d_1-d_2)}{6w_2} + \frac{d_2}{w_2}$$

These equations, (4.4)-(4.6), substituted into equation (4.3) yield

$$(4.7) \quad P_s = \frac{d_3}{2w_2}(1+\cos\theta) + \frac{d_1-d_2}{4w_2}\left(\frac{5+3\cos\theta}{6}\right) + \frac{d_2}{4w_2}$$

We may now define

TABLE 4.1

PROPORTIONS OF SLOTS CARRYING COIL SIDES FROM DIFFERENT PHASES FOR A BALANCED THREE-PHASE WINDING

Phase Difference between Currents in Top and Bottom Coil Sides	Winding Pitch p	Ratio to Total Number of Slots
$\theta^{o} = 0^{o}$	$1 \leq p \leq \frac{4}{3}$	4 - 3p
($\cos\theta = 1$)	$\frac{2}{3} \leq p \leq 1$	3p - 2
	$0 \leq p \leq \frac{2}{3}$	0
$\theta = 60^{o}$	$1 \leq p \leq \frac{4}{3}$	3p - 3
($\cos\theta = 0.50$)	$\frac{2}{3} \leq p \leq 1$	3 - 3p
	$\frac{1}{3} \leq p \leq \frac{2}{3}$	3p - 1
	$0 \leq p \leq \frac{1}{3}$	0
$\theta = 120^{o}$	$\frac{2}{3} \leq p \leq \frac{4}{3}$	0
($\cos\theta = -0.50$)	$\frac{1}{3} \leq p \leq \frac{2}{3}$	2 - 3p
	$0 \leq p \leq \frac{1}{3}$	3p
$\theta = 180^{o}$	$\frac{1}{3} \leq p \leq \frac{4}{3}$	0
($\cos\theta = -1$)	$0 \leq p \leq \frac{1}{3}$	1 - 3p

$$(4.8) \quad K_s = \frac{1+\cos\theta}{2}$$

and

$$(4.9) \quad P_s = \frac{K_s}{w_2}(d_3 + \frac{d_1}{3}) + \frac{d_1}{12w_2}(1-k_s) - \frac{d_2}{4_w}(K_s - \frac{2}{3})$$

For a closed slot, this expression must be altered as follows:

$$(4.10) \quad P_s = K_s(\frac{d_5}{w_1} + \frac{2d_4}{w_1+w_2} + \frac{d_3}{w_2}) +$$

$$\frac{d_1}{12w_2}(1-K_s) - \frac{d_2}{4w_2}(K_s - \frac{2}{3})$$

In order to apply equation (4.10), it is necessary to multiply the distinct value of K_s for the different kinds of slots by the proportion of each to find an effective value of K_s. Table 4.1, provided by Alger,[34] may be used to compute the effective value of K_s.

4.2.c. Differential Leakage Reactance (X_{ah})

The differential reactance is due to harmonic flux waves in the air gap field which induce fundamental frequency into the armature winding and thus add to the reactance in the armature. The magnetic paths for these fluxes lie in the air gap as well as in the rotor iron as illustrated by figure 4.1. The following expression and the development are, once again, provided by Alger.[35]

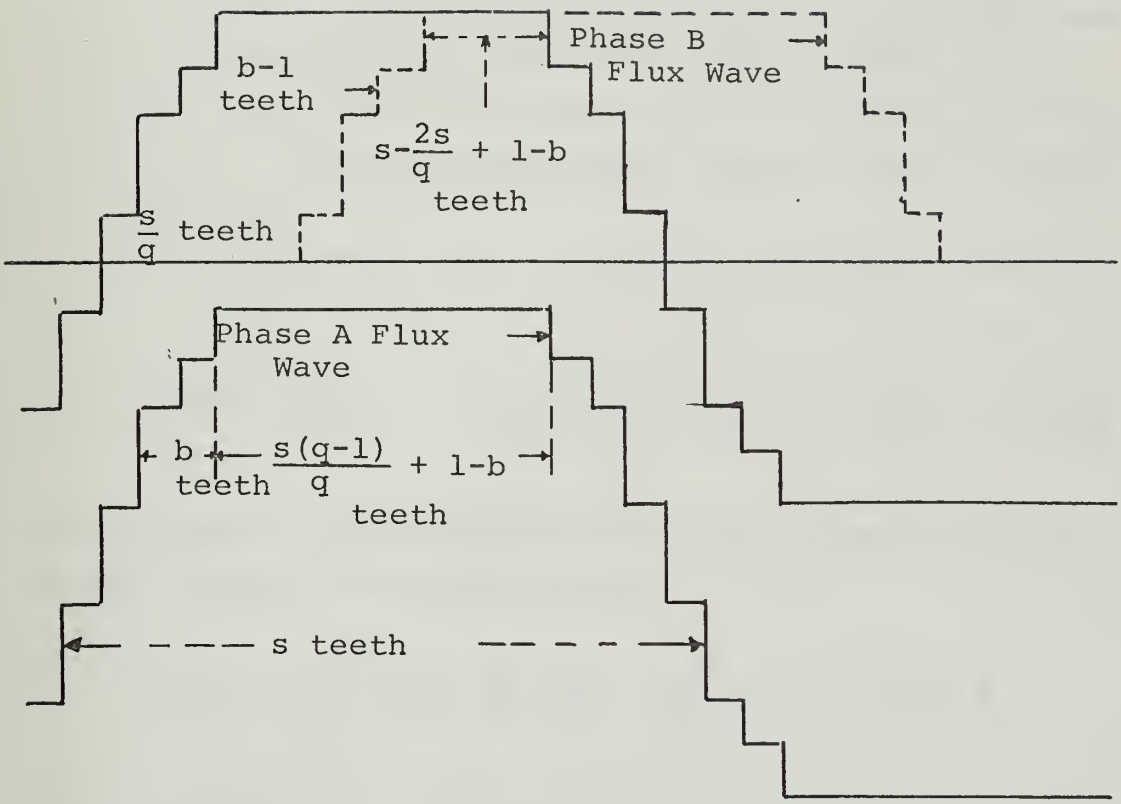

A A A A A $\bar{B}$ $\bar{B}$ $\bar{B}$ $\bar{B}$ $\bar{B}$ C C C C C $\bar{A}$ $\bar{A}$ $\bar{A}$ $\bar{A}$ $\bar{A}$ B B B B B $\bar{C}$ $\bar{C}$ $\bar{C}$

A A A $\bar{B}$ $\bar{B}$ $\bar{B}$ $\bar{B}$ $\bar{B}$ C C C C C $\bar{A}$ $\bar{A}$ $\bar{A}$ $\bar{A}$ $\bar{A}$ B B B B B $\bar{C}$ $\bar{C}$ $\bar{C}$ $\bar{C}$ $\bar{C}$

Figure 4.3 Air Gap Flux Linkages at the Instant When $I_A = -I_B : I_C = 0$

Figure 4.3 shows the stepped rectangular air gap flux wave produced by one phase, Phase A, of a q-phase winding with s slots per pole, and a coil pitch of s-b teeth. The self-linkages of phase A are the sum of the linkages due to the center teeth (teeth 4-12), carrying full flux and linking all the turns; and of the other teeth linking progressively fewer turns and carrying less flux.

The expression for the self-linkages for phase A is

$$(4.11)\quad L_{AA} = 1 - \frac{2}{3q} + \frac{9}{3s^3}(2s-3bs^2 - bq+b^39),\ 0 \leq b \leq \frac{s}{q}$$

Now, we may sum the linkages for phase B due to phase A. These linkages are expressed by

$$(4.12)\quad L_{AB} = \cos\frac{\pi}{q}\{(\frac{q-2}{q}) - \frac{bq^2}{6s^3}(b^2-1)\},\ 0 \leq b \leq \frac{s}{q}$$

For a three-phase, 60° phase belt winding, $q = 3$, $\cos(\frac{\pi}{q}) = 1/2$, the total air gap reactance is expressed by

$$(4.13)\quad L_t = L_{AA} + L_{AB} + L_{AC} = L_{AA} + 2L_{AB}$$

or

$$(4.14)\quad L_{60} = \frac{10}{9} + \frac{1}{2s^3}(4s-6b^2s-3b+3b^3),\ 0 \leq b \leq \frac{s}{3}$$

The ratio of the fundamental flux to the total generated by a single full pitch coil is $\frac{8}{\pi^2}$.

To obtain the per unit inductance due to the useful flux, we multiply this ratio by the squares of the pitch and distribution factors and by the ratio q/2 of the total field due to one phase alone which yields

$$(4.15)\quad L_s = \frac{4q^2}{\pi^2}\,\frac{\mathrm{Sin}^2\frac{\pi}{2q}\mathrm{Sin}^2\frac{2\pi(s-b)}{2s}}{S^2\mathrm{Sin}^2\frac{\pi}{2s}}$$

We now obtain the differential leakage of the winding by dividing the expression for the total leakage, equation (4.13) by equation (4.16) and substracting unity.

$$(4.16)\quad \frac{X_{ah}}{X_m} = \frac{\pi^2(20s^3+36s-54b^2s-27b+27b^3)\mathrm{Sin}^2\frac{\pi}{2s}}{486s\mathrm{Sin}^2\frac{2\pi(s-b)}{2s}} - 1, \qquad 0\leq b\leq\frac{s}{3}$$

4.2.d. End-Turn Component.

The stator end turn leakage may be determined approximately by the following expression developed by Alger.[36]

$$(4.17)\quad X_{ae} = \frac{1.84\ qfN^2D_1}{10^6p^2}\ \tan\alpha\left(\frac{p\pi-\mathrm{Sin}p\pi}{\pi}\right)\ 1-\left(\frac{.8D_2}{D_1}\right)^P$$

$$+\ .93K_{p1}^2\left(\log\frac{1.4D_1}{ds_1} - \frac{D}{D_1}\log\frac{.54D}{R}\right)\ \frac{\text{ohms}}{\text{phase}}$$

with D expressed in meters. The derivation of this expession is lengthy and the reader is referred to reference 36 for further information. As was expressed earlier, the result is approximate. The real value in using this result is that it gives some indication of the effects of

changes in dimensions in the machine on this component of leakage. Customary use of this expression is to obtain test data on a machine of similar type and to adjust the calculated value of its reactance with a constant to obtain the correct value of end turn leakage. The constant determined in this manner may then be applied to the new design.

According to Mr. Alger, it is sufficient to assume that rotor end leakage will be of approximately the same value as that in the armature. A convenient means to express the total machine leakage is to round off the first term of equation (4.7) and multiply it by 4 to obtain:

$$(4.18) \quad X_e = \frac{7fqN^2D}{p^2}(p-0.3) \text{ ohms per phase}$$

with dimensions in meters. The armature end-turn component is thus:

$$(4.19) \quad X_{ae} = \frac{X_e}{2} ,$$

and the total armature leakage is

$$(4.20) \quad X_a = X_{as} + X_{at} + X_{ah} + X_{ae}$$

4.3. Field Leakage Reactance.

The field leakage reactance is composed of the sum of a slot-leakage component and an end-turn leakage component. The end-turn leakage referred to the stator may be estimated by equation (4.18).

$$(4.21) \quad X_{fe} = \frac{X_e}{2}$$

The field slot-leakage is calculated in the same manner as is the stator slot leakage (Section 4.2.b.) Equation (4.3) may be used to express the field slot leakage as an inductance.

$$(4.22) \quad L_{fs} = (N_s)^2 (L)(P_s)(4\pi \times 10^{-7}) \ \frac{\text{henrys}}{\text{slot}}$$

where N_s = turns per slot

Since the field slots contain fewer turns in the slots nearest the pole face, Equation (4.22) must be applied separately to each slot. The total field leakage inductance is determined by summing the contribution of all slots.

In order to refer the value for L_{fs} to the stator, we may use a turn ratio which results from a per unit system developed by Concordia.[37] Concordia's expression for the flux relations of a synchronous machine's main field and armature circuits in d, q variables, ignoring damper winding currents, are:[38]

$$(4.23) \quad \lambda_d = -L_d i_d + M i_f$$

$$\lambda_q = -L_q i_q$$

$$\lambda_f = \frac{3}{2} M i_d + L_f i_f$$

Concordia defines $I_f = \frac{2}{3} i_f$ which substituted in equation (4.23) yields:

$$\lambda_d = -L_d i_d + \frac{3}{2} M I_f$$

$$(4.24) \quad \lambda_q = -L_q i_q$$

(4.24 con't) $$\lambda_f = -\frac{3}{2} M i_d + \frac{3}{2} L_f I_f$$

where

$$(4.25) \qquad L_d = L_{ad} + \ell_a$$

and $L_{ad} i_d$ is the magnitude of the first harmonic flux. If we require that in per unit, all rotor and armature mutual flux be equal to the per unit value of this first harmonic flux and choose rated voltage and current as base voltage (V_o) and current (I_o), we have defined the following base relationships.

$$(4.26) \qquad L_{ad}\text{p.u.} = \omega L_{ad} \frac{I_o}{V_o} = \omega \frac{3}{2} M \frac{I_{fo}}{V_o}$$

$$(4.27) \qquad I_{fo} = \frac{2}{3} \frac{L_{ad}}{M} I_o$$

$$(4.28) \qquad X_f\text{p.u.} = \omega \frac{3}{2} L_f \frac{I_{fo}}{V_{fo}}$$

which combined yield the result

$$(4.29) \qquad X_f\text{p.u.} = \frac{\omega \frac{2}{3} L_f}{Z_o} \left(\frac{L_{ad}}{M}\right)^2$$

where

$$(4.30) \qquad M = \frac{\sqrt{2} E_f}{\omega I_f} \text{ henry}$$

and[39]

$$(4.31) \qquad L_{ad} = \frac{4qN^2 K_p^2 K_d^2 DL}{P^2 G 10^7}$$

TABLE 4.2

REACTANCE CALCULATIONS IN PER UNIT

	BIG SANDY (Manufacturer)	BIG SANDY Calculated	BIG SANDY MODEL Calculated
Synchronous Reactance	2.22	2.41	2.094*
Mutual Reactance (L_{ad})	2.04	2.27	2.070
Armature Leakage	.18	.142	.024
Tooth-Top	--	.011	--
Slot	--	.104	.007
End-Turn	--	.02	.002
Differential	--	.007	.015
Field Leakage	.05	.10	.009
Slot	--	.08	.007
End-Turn	--	.02	.002

*External Reactance Not Included

4.4. Estimation of External Reactance Correction for BIG SANDY model.

The procedures discussed in sections 4.2-4.3 were used to calculate the leakage reactances for BIG SANDY and the BIG SANDY model. The results of the calculations are tabulated in table 4.2. Note that the values calculated for BIG SANDY differ appreciably from the reactance values calculated by the Manufacturer, General Electric Company, in two areas. First, the value of L_{ad} from equation (4.30) is too large. This may possibly be explained by the fact that in the generator the end regions are shielded by highly conducting materials in order to protect the stator laminations from axial fields created by the end turns; this shielding tends to reduce the self and mutual reactance achieved in the generator and may be accounted for in the G. E. calculation.[41]

The second area of difference is in the field leakage calculations. The values determined using the procedure developed in section 4.3 are too high. This error may possibly be accounted for if we compare the total leakage, armature plus field. Thus, total leakage reactance calculated for BIG SANDY is quite close to the values provided by G. E. This total leakage reactance is approximately equal to the transient reactance which is unaffected by the turns ratio which results from the per unit system used. The difference observed in the values for field leakage may be due then to use of a different per unit system by G. E. from that used in section 4.3.

In view of the observed discrepancies just discussed, the necessary field and armature reactance corrections to match the BIG SANDY leakage reactance may not be accurately

calculated at this time. It will be necessary to conduct tests on the physical model to establish these parameters. It is clear from the results that nearly all the leakage must be added externally. The approximately inductances which must be added in the armature and field are 25 mh and 37 mh respectively.

CHAPTER 5

CONCLUSIONS

5.1. Modified Design Conclusions and Recommendations.

The modeling project of the Electric Power Systems Laboratory has suffered from the lack of a working model to verify and improve theory developed to date. It is believed that the model to be constructed from the design developed in this thesis will meet this need.

The reduced stator and rotor slot widths should be effective in minimizing eddy current losses which in turn should permit thorough testing and evaluation of the model and the modeling concept.

Two areas where additional research is needed are indicated. First of all, a thorough study of the effects of the holes in the rotor laminations on rotor saturation characteristics is required. The validity of using the teledeltos analog to predict saturation effects remains to be proved.

Secondly, the effects of rotor damper circuits, of which there are an infinite number, on the machine reactances must be investigated. The leakage reactance calculations undertaken in Chapter 4 were valuable as far as indicating that the closed slots combined with the small air gap would not create a situation which would result in excessive leakage, but the results are incomplete as far as accurately determining leakage reactance. This is due to the failure to include the effects of damper circuits and also because of the inexact procedure used to estimate end-turn leakage.

5.2. Applicability of Modeling Procedure to Naval Electrical Systems.

The modeling procedure used in this thesis is not applicable for the design of a model for a ship service generator of the type currently in use aboard modern U. S. Navy vessels. The ship service generators used today are primarly 6-pole, 1200 rpm units with laminated rotors. In view of the increasing use of gas turbines on board ships of the Navy, however, it is conceivable that in the not too distant future, 2-pole 3600 rpm units with solid steel forged rotors will be utilized. Should this happen, the procedure would be applicable.

The same justifications for physically modeling the large generators would also be applicable to a similar system if it is introduced aboard ship. In fact, a stronger case for physically reproducing non-linear electromagnetic phenomena associated with a generator could be made for a shipboard system because of the short transmission systems and closely coupled loads. The transient response of a generator is of much more importance in such a system.

REFERENCES

1. H. H. Woodson, "Progress Report on the AEP System Model Feasibility Study, "Report No. 3, Power Systems Engineering Group, School of Engineering, M.I.T., Cambridge, Mass., November, 1967.

2. H. H. Woodson and W. C. Euerle, "Second Progress Report on the AEP System Model Feasibility Study," Report No. 9, Power Systems Engineering Group, School of Engineering, M.I.T., Cambridge, Mass., July, 1968, p. 1.

3. Ibid., p.4.

4. A. S. Pasquale, "A Scale Model of a Large Steam Turbine Generator," SM Thesis, Department of Electrical Engineering, M.I.T., Cambridge, Mass., July, 1968.

5. H. H. Woodson and W. C. Euerle, "Third Progress Report on the AEP Systems Model Feasibility Study," Report No. 18, Power Systems Engineering Group, School of Engineering, M.I.T., Cambridge, Mass., September, 1969, p. 15.

6. Ibid., pp.16-19.

7. Power Systems Engineering Group Report No. 3, pp.2-5.

8. Ibid.

9. Power Systems Engineering Group Report No. 9, p.5.

10. Power Systems Engineering Group Report No. 18, p.24.

11. H. H. Woodson, "Summary of Design Procedure for Turbogenerator Models," Memorandum to Prof. G. L. Wilson, July 22, 1971.

12. S. D. Umans, "Design, Construction and Testing of a Scale Model of a Cylindrical Rotor, Steam Turbine Generator," SM Thesis, Department of Electrical Engineering, M.I.T., Cambridge, Mass., June, 1972.

13. J. Greig and K. Sathirakul, "Pole-Face Losses in Alternators," The IEEE Monograph No. 40, IEEE, October, 1960.

14. W. J. Gibbs, "Tooth-Ripple Losses in Unwound Pole-Shoes," Journal I.E.E., Vol. 94, Part II, February, 1947, p.2.

15. D. K. Cheng, Analysis of Linear Systems, Addison-Wesley Publishing Co., Reading, Mass., 1959, p.141.

16. S. D. Umans SM Thesis.

17. Ibid.

18. Ibid.

19. Ibid.

20. A. E. Fitzgerald, Charles Kingsley, Jr., and A. Kusko, Electric Machinery, Third Edition, McGraw-Hill Book Co., New York, N.Y., 1961, p.149.

21. S. D. Umans SM Thesis.

22. Ibid.

23. H. E. Haller III, "A Scale Model of a Steam Turbine Generator," SM Thesis, Department of Electrical Engineering, M.I.T., Cambridge, Mass., May, 1970,p.46.

24. S. D. Umans SM Thesis.

25. W. C. Euerle, Lab Notebook No. 2, Experiment No. 1, January, 1965.

26. H. E. Haller III, SM Thesis, p.41.

27. S. D. Umans, SM Thesis.

28. H. H. Woodson Memorandum, pp.6,7

29. Ibid., p.21.

30. S. D. Umans SM Thesis

31. M. E. Talaat, "A New Approach to the Calculation of Synchronous Machine Reactances-Part II,", A.I.E.E. Transactions Part II, Vol.75, 1956, pp.317-327.

32. Ibid.

33. P. L. Alger, The Nature of Induction Machines, Gordon and Breach Science Publishers, New York, N.Y., 1965, pp.201-208.

34. Ibid.,p.205

35. Ibid., pp.209-216.

36. Ibid., p.243

37. C. Concordia, Synchronous Machines, Theory and Performance, John Wiley and Sons, Inc., New York, N.Y., 1951, pp.6-22.

38. J. L. Kirtley, Personal Notes on Concordia's Formulation, April 12, 1972.

39. P. L. Alger, The Nature of Induction Machines,p.201.

40. J. L. Kirtley, personal communication.

134541

Thesis
W596 Williams
Modified design of a scale model of a cylindrical rotor, steam turbine generator.
DISPLAY

134541

Thesis
W596 Williams
Modified design of a scale model of a cylindrical rotor, steam turbine generator.

thesW596
Modified design of a scale model of a cy
3 2768 000 99837 1
DUDLEY KNOX LIBRARY